Frontiers of Information Technology & Electronic Engineering
www.jzus.zju.edu.cn; engineering.cae.cn; www.springerlink.com
ISSN 2095-9184 (print); ISSN 2095-9230 (online)
E-mail: jzus@zju.edu.cn

Control strategy for gait transition of an underactuated 3D bipedal robot*

Hai-hui YUAN[1,2], Yi-min GE[1,2], Chun-biao GAN‡[1,2]

[1]*State Key Laboratory of Fluid Power and Mechatronic Systems, School of Mechanical Engineering, Zhejiang University, Hangzhou 310027, China*

[2]*Key Laboratory of Advanced Manufacturing Technology of Zhejiang Province, School of Mechanical Engineering, Zhejiang University, Hangzhou 310027, China*

E-mail: hh_yuan@zju.edu.cn; geyimin@zju.edu.cn; cb_gan@zju.edu.cn

Received Apr. 3, 2018; Revision accepted June 17, 2018; Crosschecked Aug. 9, 2019

Abstract: Significant research interest has recently been attracted to the study of bipedal robots due to the wide variety of their potential applications. In reality, bipedal robots are often required to perform gait transitions to achieve flexible walking. In this paper, we consider the gait transition of a five-link underactuated three-dimensional (3D) bipedal robot, and propose a two-layer control strategy. The strategy consists of a unique, event-based, feedback controller whose feedback gain in each step is updated by an adaptive control law, and a transition controller that guides the robot from the current gait to a neighboring point of the target gait so that the state trajectory can smoothly converge to the target gait. Compared with previous works, the transition controller is parameterized and its control parameters are obtained by solving an optimization problem to guarantee the physical constraints in the transition process. Finally, the effectiveness of the control strategy is illustrated on the underactuated 3D bipedal robot.

Key words: Gait transition; Underactuated three-dimensional biped; Event-based feedback controller; Adaptive control law

https://doi.org/10.1631/FITEE.1800206 **CLC number:** TP242

1 Introduction

The study of bipedal robots is fascinating due to the wide variety of potential applications in the areas of military use, disaster rescue, and family service (Hirose and Ogawa, 2007; Kaneko et al., 2015; Yanco et al., 2015). In the last few decades, a lot of successful prototypes have been designed, such as ASIMO (Hirose and Ogawa, 2007), HRP (Kaneko et al., 2011), and HUBO (Park et al., 2007). These high-degree-of-freedom robots address the challenge of bipedal balance by careful regulation of their zero-moment point (ZMP) (Vukobratović and Borovac, 2004). Although the full-actuation approach is very effective in physical environments, it is relatively conservative because it requires bipedal robots be balanced at each state. In addition, the full-actuation approach tends to consume more power (Collins et al., 2005).

Recently, underactuated bipedal robots have attracted significant research interest (Gregg and Righetti, 2013; Ames et al., 2014; Montano et al., 2017), and a lot of successful control strategies have been proposed. Ames (2014) proposed a human-inspired control approach for bipedal walking that uses human data. Li et al. (2015) proposed

‡ Corresponding author

* Project supported by the National Natural Science Foundation of China (Nos. 91748126, 11772292, and 51521064)

ORCID: Chun-biao GAN, http://orcid.org/0000-0002-6597-5605

hip strategies for underactuated bipeds subject to external forces. Sreenath et al. (2013) proposed an active force control method to achieve fast and stable running of the bipedal robot MABEL. Yi and Lin (2015) developed a running control law for an underactuated planar biped. Tang et al. (2015) proposed a discrete transverse linearization method to achieve stable walking of a three-dimensional (3D) compasslike biped. Chevallereau et al. (2009) proposed an event-based control method to achieve stable walking of a five-link underactuated 3D biped. Hamed and Grizzle (2014) further developed the event-based control strategy into a time-invariant one-step hybrid control scheme on the basis of right-left symmetry, linear matrix inequalities (LMIs), and robust optimal control (ROC). Although exhibiting very efficient energy and natural dynamics, these control strategies focus mainly on the stabilization of underactuated bipedal robots on one single periodic gait. In reality, bipedal robots are often required to perform gait transitions to achieve flexible walking, such as controlling the walking speed (Hobbelen and Wisse, 2008; Moon et al., 2016), changing the walking direction (Shih et al., 2012), or regulating the step length (Hu et al., 2011). Nevertheless, because there are not enough actuators, the gait characteristics of an underactuated biped cannot be directly controlled or preplanned as they can in fully actuated robots (Chevallereau et al., 2009; Geng, 2014). Therefore, it is a nontrivial task for underactuated bipeds to realize precise or smooth transition from one gait to another.

Currently, studies on gait transition of underactuated bipedal robots are relatively limited, and they focus mainly on planar robots. Hobbelen and Wisse (2008) proposed a strategy combining feedforward actuation adjustment with step-to-step speed feedback to regulate the walking speed of a planar biped with passive knees. Geng (2014) proposed a two-level control structure consisting of a walking controller and a model predictive controller to regulate the walking speed of a five-link planar biped. Yi et al. (2014) proposed a strategy combining transitional control with event-based control to achieve variable speed running on a four-link planar biped. Da et al. (2016) and Nguyen et al. (2017) proposed a novel gait transition method by combining a virtual constraint approach with an interpolation method, and the results were validated experimentally. In Da et al. (2017), this gait transition method was further improved with the supervised learning approach. In another very interesting study, Yang et al. (2009) considered the gait transitions between a set of previously designed gaits to achieve stable aperiodic walking, where smooth transition is achieved by a hierarchical control structure consisting of an individual controller and a one-step transition controller that could guide the biped to an expected final configuration.

Compared with underactuated planar bipeds, 3D bipeds have more degrees of underactuation and their stabilization problems are more difficult, which make the control of gait transition more challenging. To the best of our knowledge, few researchers have focused on gait transitions of 3D cases. Here, to achieve stable and smooth gait transition of an underactuated 3D biped, we propose a two-layer control strategy that consists of an event-based feedback controller and a transition controller. The event-based feedback controller is designed to achieve stability of the target gait, and the transition controller is designed to guide the robot from the current gait to a neighboring point of the target gait. To guarantee the physical constraints in the transition process, the transition controller is parameterized and its control parameters are obtained by solving an optimization problem.

2 Preliminaries

The 3D biped considered is depicted in Fig. 1. Here, q_0, q_1, and q_2 are the yaw, pitch, and roll angles of the stance leg, respectively; q_3 and q_8 are the relative joint angles of the stance-leg knee and swing-leg knee, respectively; q_4 and q_5 are the relative joint angles of the stance-leg hip; q_6 and q_7 are the relative joint angles of the swing-leg hip. Angles q_2, q_5, and q_6 are in the frontal plane, while q_1, q_3, q_4, q_7, and q_8 are in the sagittal plane. Angles q_0, q_1, and q_2 are underactuated due to passive contact, while $\boldsymbol{q}_a = [q_3, q_4, \ldots, q_8]^{\mathrm{T}}$ are independently actuated. Angles $q_{0,\mathrm{sw}}$, $q_{1,\mathrm{sw}}$, and $q_{2,\mathrm{sw}}$ denote the relative angles of the swing-leg shin, and they can be calculated by kinematic relationships. This robot consists of five rigid links connected by revolute joints: a torso and two symmetric legs. For simplicity, each link is modeled by a point mass at its center.

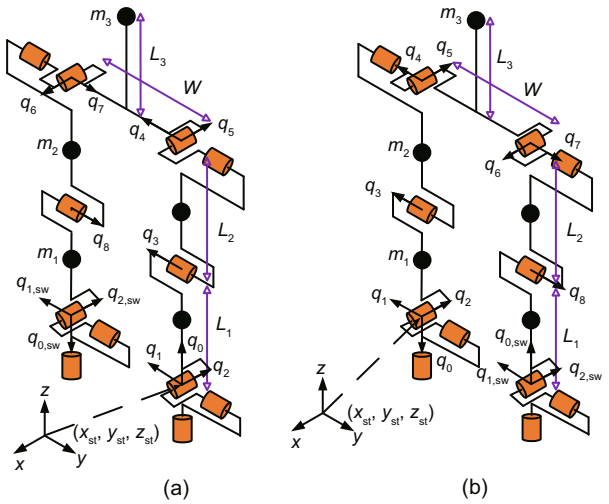

Fig. 1 Model of the three-dimensional (3D) five-link biped. The robot is supporting on the left (a) and right (b) legs, respectively

2.1 Hybrid model of bipedal walking

We consider the most important and simple form of 3D bipedal walking, i.e., symmetric walking. Moreover, the 3D bipedal walking is assumed to consist of two alternating phases of motion: single support and double support. It is further assumed that the double support phase is instantaneous and occurs when the swing leg impacts the ground. As a result, the 3D bipedal robot is modeled as a hybrid system.

In the single support phase, the yaw rotation q_0 is assumed to be inhibited by friction, and thus $\boldsymbol{q} = [q_1, q_2, \dots, q_8]^{\mathrm{T}}$ are defined as the generalized coordinates. Based on the customary Lagrangian method, the dynamic model for the 3D biped in the single support phase can be obtained as

$$\boldsymbol{D}_v(\boldsymbol{q})\ddot{\boldsymbol{q}} + \boldsymbol{H}_v(\boldsymbol{q}, \dot{\boldsymbol{q}}) = \boldsymbol{B}\boldsymbol{u}_v, \tag{1}$$

where the subscript $v \in \{1, 2\}$ denotes the left or right support phase, $\boldsymbol{D}_v(\boldsymbol{q})$ is the positive-definite 8×8 mass-inertia matrix, $\boldsymbol{H}_v(\boldsymbol{q}, \dot{\boldsymbol{q}})$ is the 8×1 vector of Coriolis and gravity terms, $\boldsymbol{B}$ is a full-rank, constant matrix indicating whether a joint is actuated or not, and $\boldsymbol{u}_v$ is the 6×1 vector of the input torques. Defining the state variables as $\boldsymbol{x}_v = [\boldsymbol{q}, \dot{\boldsymbol{q}}]^{\mathrm{T}}$, model (1) can be rewritten as

$$\dot{\boldsymbol{x}}_v = \boldsymbol{f}_v(\boldsymbol{x}_v) + \boldsymbol{g}_v(\boldsymbol{x}_v)\boldsymbol{u}_v, \tag{2}$$

where

$$\boldsymbol{f}_v(\boldsymbol{x}_v) = \begin{bmatrix} \dot{\boldsymbol{q}} \\ -\boldsymbol{D}_v^{-1}(\boldsymbol{q})\boldsymbol{H}_v(\boldsymbol{q}, \dot{\boldsymbol{q}}) \end{bmatrix},$$

$$\boldsymbol{g}_v(\boldsymbol{x}_v) = \begin{bmatrix} \boldsymbol{0} \\ \boldsymbol{D}_v^{-1}(\boldsymbol{q})\boldsymbol{B} \end{bmatrix}.$$

During the double support phase, $\boldsymbol{q}_e = [x_{\mathrm{st}}, y_{\mathrm{st}}, z_{\mathrm{st}}, q_0, q_1, \dots, q_8]^{\mathrm{T}}$ are defined as the generalized coordinates, where $(x_{\mathrm{st}}, y_{\mathrm{st}}, z_{\mathrm{st}})$ are the Cartesian coordinates of the stance foot. Next, under assumptions that are analogous to those in Grizzle et al. (2001), the impact model for the double support phase can be obtained as

$$\begin{bmatrix} \dot{\boldsymbol{q}}_{v,e}^{+} \\ \boldsymbol{F}_{v,\mathrm{sw}} \end{bmatrix} = \begin{bmatrix} \boldsymbol{D}_{v,e} & -\boldsymbol{E}_{v,\mathrm{sw}}^{\mathrm{T}} \\ \boldsymbol{E}_{v,\mathrm{sw}} & \boldsymbol{0} \end{bmatrix}^{-1} \begin{bmatrix} \boldsymbol{D}_{v,e}\dot{\boldsymbol{q}}_{v,e}^{-} \\ \boldsymbol{0} \end{bmatrix}, \tag{3}$$

where $\dot{\boldsymbol{q}}_{v,e}^{-}$ and $\dot{\boldsymbol{q}}_{v,e}^{+}$ are the extended velocities before and after the impact respectively, $\boldsymbol{F}_{v,\mathrm{sw}}$ is the impulsive reaction force on the swing leg at the contact point, $\boldsymbol{D}_{v,e}$ is the generalized mass-inertia matrix, and $\boldsymbol{E}_{v,\mathrm{sw}} = \partial/\partial\boldsymbol{q}_e[x_{\mathrm{sw}}, y_{\mathrm{sw}}, z_{\mathrm{sw}}, q_{0,\mathrm{sw}}]^{\mathrm{T}}$ is the Jacobian for the position of the swing foot and its orientation in the x-y plane. After the impact, the coordinates $[q_{1,\mathrm{sw}}, q_{2,\mathrm{sw}}, q_8, q_7, \dots, q_3]$ are relabeled as $[q_1, q_2, \dots, q_8]$, as shown in Fig. 1. Then by combining the coordinate relabeling and the impact model, the dynamic model for the double support is given by

$$\boldsymbol{x}_{v+1}^{+} = \boldsymbol{\Delta}_v^{v+1}(\boldsymbol{x}_v^{-}) = \begin{bmatrix} \boldsymbol{\Delta}_{v,q}(\boldsymbol{q}^{-}) \\ \boldsymbol{\Delta}_{v,\dot{q}}(\boldsymbol{q}^{-}, \dot{\boldsymbol{q}}^{-}) \end{bmatrix}, \tag{4}$$

where $\boldsymbol{x}_{v+1}^{+} = [\boldsymbol{q}_{v+1}^{+}, \dot{\boldsymbol{q}}_{v+1}^{+}]^{\mathrm{T}}$ is the initial state of the next step and $\boldsymbol{x}_v^{-} = [\boldsymbol{q}_v^{-}, \dot{\boldsymbol{q}}_v^{-}]^{\mathrm{T}}$ is the final state of the current step. Similar to Grizzle et al. (2014), considering the periodicity of the 3D bipedal walking, we use the notation $v + 1 = 1$ for $v = 2$.

From Eqs. (2) and (4), the complete hybrid system of the 3D bipedal robot can be expressed as

$$\boldsymbol{\Sigma} := \begin{cases} \dot{\boldsymbol{x}}_1 = \boldsymbol{f}_1(\boldsymbol{x}_1) + \boldsymbol{g}_1(\boldsymbol{x}_1)\boldsymbol{u}_1, & \boldsymbol{x}_1 \notin \boldsymbol{S}_1^2, \\ \boldsymbol{x}_2^{+} = \boldsymbol{\Delta}_1^2(\boldsymbol{x}_1^{-}), & \boldsymbol{x}_1 \in \boldsymbol{S}_1^2, \\ \dot{\boldsymbol{x}}_2 = \boldsymbol{f}_2(\boldsymbol{x}_2) + \boldsymbol{g}_2(\boldsymbol{x}_2)\boldsymbol{u}_2, & \boldsymbol{x}_2 \notin \boldsymbol{S}_2^1, \\ \boldsymbol{x}_1^{+} = \boldsymbol{\Delta}_2^1(\boldsymbol{x}_2^{-}), & \boldsymbol{x}_2 \in \boldsymbol{S}_2^1, \end{cases} \tag{5}$$

where $\boldsymbol{S}_v^{v+1} = \{\boldsymbol{x}_v | z_{\mathrm{sw}}(\boldsymbol{x}_v) = 0,\ x_{\mathrm{sw}}(\boldsymbol{x}_v) > 0\}$ $(v = 1, 2)$ denotes the switching surface. Moreover, for symmetric walking, we have

$$\boldsymbol{x}_1(t) = \boldsymbol{\Psi}\boldsymbol{x}_2(t), \tag{6}$$

where $\boldsymbol{\Psi} = \begin{bmatrix} \boldsymbol{\Pi} & \boldsymbol{0}_{8\times8} \\ \boldsymbol{0}_{8\times8} & \boldsymbol{\Pi} \end{bmatrix}$ and

$$\boldsymbol{\Pi} = \mathrm{diag}(1, -1, 1, 1, -1, -1, 1, 1).$$

Therefore, for simplicity of analysis, the dynamic model (1) is simplified as

$$\boldsymbol{\Sigma} := \begin{cases} \dot{\boldsymbol{x}}_1 = \boldsymbol{f}_1(\boldsymbol{x}_1) + \boldsymbol{g}_1(\boldsymbol{x}_1)\boldsymbol{u}_1, & \boldsymbol{x}_1 \notin \boldsymbol{S}_1^2, \\ \boldsymbol{x}_1^+ = \boldsymbol{\Delta}(\boldsymbol{x}_1^-), & \boldsymbol{x}_1 \in \boldsymbol{S}_1^2, \end{cases} \tag{7}$$

where $\boldsymbol{\Delta} = \boldsymbol{\Psi}\boldsymbol{\Delta}_1^2$. In the actual implementation, the bipedal walking with the right stance leg can be managed using the symmetry property (6) (Chevallereau et al., 2009; Hamed and Grizzle, 2014).

2.2 Periodic gait planning using virtual constraints

The virtual constraint approach (Westervelt et al., 2007; Chevallereau et al., 2009; Freidovich et al., 2009) is the most basic tool for periodic gait planning of underactuated systems. In this approach, the periodic gait planning of an underactuated system can be transformed into a parameter optimization process to find the virtual constraint coefficients that define a periodic gait. Here, the virtual constraints for the underactuated 3D biped are expressed as

$$\boldsymbol{y} = \boldsymbol{q}_a - \boldsymbol{h}_{\mathrm{d}}(\boldsymbol{\alpha}, \theta), \tag{8}$$

where $\boldsymbol{q}_a = [q_3, q_4, \ldots, q_8]^{\mathrm{T}}$ denote the controlled joints, $\theta = -q_1 - 0.5q_3$ is a quantity that strictly increases along a typical walking gait, and $\boldsymbol{h}_{\mathrm{d}}(\boldsymbol{\alpha}, \theta)$ is the desired evolution of the controlled joints as a function of θ with parameters $\boldsymbol{\alpha}$. Here, $\boldsymbol{h}_{\mathrm{d}}(\boldsymbol{\alpha}, \theta)$ is designed as a form of Bezier polynomial of degree three, i.e.,

$$\boldsymbol{h}_{\mathrm{d}}(\boldsymbol{\alpha}, \theta) = \sum_{k=0}^{3} \boldsymbol{\alpha}_k \frac{3!}{k!(3-k)!} s^k (1-s)^{3-k}, \tag{9}$$

where $s = (\theta - \theta_{\mathrm{f}})/(\theta_{\mathrm{f}} - \theta_{\mathrm{ini}})$ is the normalized independent variable, the subscripts "ini" and "f" denote "initial" and "final" respectively, and the coefficients $\boldsymbol{\alpha}_k$ are 6×1 vectors of real numbers and can be deduced from the final state $\boldsymbol{x}^- = [\boldsymbol{q}^-, \dot{\boldsymbol{q}}^-]^{\mathrm{T}}$. Therefore, the search for a periodic gait can be cast as a constrained nonlinear optimization problem: find the optimization parameters prescribing the final state $\boldsymbol{x}^-$ that minimizes the integral-squared torque per step length:

$$J = \frac{1}{L_{\mathrm{step}}} \int_0^T ||\boldsymbol{u}_1(t)||^2 \mathrm{d}t, \tag{10}$$

where T and L_{step} are the step duration and step length respectively, subject to the physical constraints of bipedal walking and some other constraints that reflect different requirements (Chevallereau et al., 2009; Dehghani et al., 2015).

The above optimization process is performed in MATLAB with the Patternsearch function in the optimization toolbox. Because the criterion being optimized has many local minima and the optimization technique used is local, the optimization results depend on the initial set of the optimization parameters.

3 A two-layer control strategy for gait transition

To clarify the control strategy, this section focuses on the gait transition between two periodic gaits. Similar analysis can be performed for the transition between other gaits in a gait library.

3.1 Overview of the control strategy

Mathematically, the gait transition between two periodic gaits is actually the transition from one periodic orbit of the dynamic model to another. Suppose that two periodic gaits have been obtained by the virtual constraint approach, and the robot is expected to transit from gait 2 to gait 1 (Fig. 2), where $\boldsymbol{S}_1^2$ denotes the switching hyper-surface of the dynamic model (7), and $\Delta(\boldsymbol{S}_1^2)$ denotes the hyper-surface after the discrete phase. Gait 2 and gait 1 are represented by the green and red periodic orbits, respectively. $(\boldsymbol{x}^+)_l$ and $(\boldsymbol{x}^-)_l$ $(l = 1, 2)$ are the desired initial and final states for the gaits, respectively. The dashed curve represents the discrete phases. The ring area around gait 1 represents the neighboring

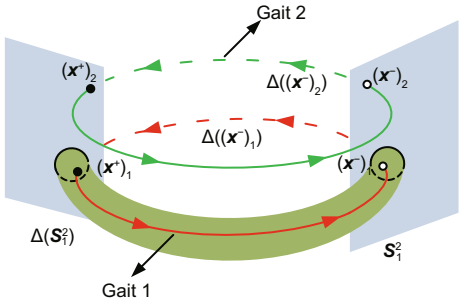

Fig. 2 Illustration of two periodic gaits for gait transition. References to color refer to the online version of this figure

area where the state trajectory can smoothly converge to gait 1. To achieve a stable and smooth transition, we propose a two-layer control strategy consisting of an event-based feedback controller and a transition controller. The event-based feedback controller is designed to achieve stability of gait 1, and the transition controller is designed to guide the robot from gait 2 to a neighboring point of gait 1. The control strategy will be described in detail in the next subsection.

3.2 Event-based feedback controller

The event-based control method (Chevallereau et al., 2009; Hamed and Grizzle, 2014) has proved to be an effective tool for the stabilization of underactuated 3D bipeds. In this subsection, we will develop a novel event-based feedback controller. Compared with previous works, the feedback gain of the controller in each step is not constant, but it is updated by an adaptive control law to achieve an optimal performance in terms of the balance between the convergence rate and input energy.

1. Control objective

From Chevallereau et al. (2009), for underactuated 3D bipeds, the stability of the closed-loop system can be dramatically improved through a judicious choice of the control output. The effectiveness of the choice of the output has also been shown in Hamed et al. (2016) and Griffin and Grizzle (2017). Here, to introduce the present feedback controller in a clear way, we simply use the actuated joints as the controlled variables for the output. Specifically, the feedback controller in the k^{th} step is constructed as

$$\begin{aligned}\boldsymbol{\Gamma}(\boldsymbol{x}_1,\boldsymbol{\beta}_k)=\boldsymbol{u}_1^*(\boldsymbol{x}_1,\boldsymbol{\beta}_k)-(\boldsymbol{L}_{g_1}\boldsymbol{L}_{f_1}\boldsymbol{y}_1(\boldsymbol{x}_1,\boldsymbol{\beta_k}))^{-1}\\ \cdot\left(\frac{K_P}{\varepsilon^2}\boldsymbol{y}_1(\boldsymbol{x}_1,\boldsymbol{\beta}_k)+\frac{K_D}{\varepsilon}\dot{\boldsymbol{y}}_1(\boldsymbol{x}_1,\boldsymbol{\beta}_k)\right),\end{aligned}\tag{11}$$

where

$$\boldsymbol{u}_1^*(\boldsymbol{x}_1,\boldsymbol{\beta}_k)=-(\boldsymbol{L}_{g_1}\boldsymbol{L}_{f_1}\boldsymbol{y}_1(\boldsymbol{x}_1,\boldsymbol{\beta}_k))^{-1}\boldsymbol{L}_{f_1}^2\boldsymbol{y}_1(\boldsymbol{x}_1,\boldsymbol{\beta}_k),$$

$\boldsymbol{L}_{g_1}$ and $\boldsymbol{L}_{f_1}$ are the Lie derivatives (Westervelt et al., 2007), $K_P>0$, $K_D>0$, and ε is a sufficiently small positive constant. In addition, $\boldsymbol{y}_1(\boldsymbol{x}_1,\boldsymbol{\beta}_k)$ is the parameterized output for the control system with a vector of adjustable parameters $\boldsymbol{\beta}_k\in\boldsymbol{\Xi}$ ($\boldsymbol{\Xi}\in\mathbb{R}^6$), which is designed as

$$\boldsymbol{y}_1(\boldsymbol{x}_1,\boldsymbol{\beta}_k)=\boldsymbol{q}_a-\boldsymbol{h}_e(\theta)-\boldsymbol{h}_s(\theta,\boldsymbol{\beta}_k).\tag{12}$$

Here, $\boldsymbol{h}_e(\theta)$ is the Bezier polynomial of degree three with the Bezier coefficients determined from the actual initial state and the desired final state, and $\boldsymbol{h}_s(\theta,\boldsymbol{\beta}_k)$ is an additional term to shift the eigenvalues of the Poincaré map which is designed to be a fifth-order polynomial of θ such that

$$\begin{cases}\boldsymbol{h}_s(\theta_{\text{ini}},\boldsymbol{\beta}_k)=\boldsymbol{0},\\ \dfrac{\partial\boldsymbol{h}_s}{\partial\theta}(\theta_{\text{ini}},\boldsymbol{\beta}_k)=\boldsymbol{0},\\ \boldsymbol{h}_s((\theta_{\text{ini}}+\theta_{\text{f}})/2,\boldsymbol{\beta}_k)=\boldsymbol{\beta}_k,\\ \boldsymbol{h}_s(\theta,\boldsymbol{\beta}_k)\equiv\boldsymbol{0},\quad 0.1\theta_{\text{ini}}+0.9\theta_{\text{f}}\le\theta\le\theta_{\text{f}}.\end{cases}\tag{13}$$

Moreover, the continuity of position, velocity, and acceleration is ensured at $\theta=0.1\theta_{\text{ini}}+0.9\theta_{\text{f}}$.

With the additional term $\boldsymbol{h}_s(\theta,\boldsymbol{\beta}_k)$, the Poincaré map $\boldsymbol{P}:\boldsymbol{S}_1^2\times\boldsymbol{\Xi}\to\boldsymbol{S}_1^2$ induces a nonlinear discrete-time system:

$$\boldsymbol{x}_k=\boldsymbol{P}(\boldsymbol{x}_{k-1},\boldsymbol{\beta}_k),\tag{14}$$

where the subscript k represents the step number. Here, the controller parameter $\boldsymbol{\beta}_k$ in the k^{th} step is updated by

$$\boldsymbol{\beta}_k=-\boldsymbol{K}_{n_k}(\boldsymbol{x}_{k-1}-\boldsymbol{x}^*),\tag{15}$$

where $\boldsymbol{x}^*$ is the fixed point of $\boldsymbol{P}$, $\boldsymbol{K}_{n_k}$ the feedback gain to be determined in the k^{th} step, and n_k a positive integer.

Because $\boldsymbol{\beta}_k$ is designed to be a function of $\boldsymbol{x}_{k-1}$, the Poincaré map $\boldsymbol{P}$ in the k^{th} step can be represented by the Poincaré map $\boldsymbol{P}_{n_k}:\boldsymbol{S}_1^2\to\boldsymbol{S}_1^2$, and

$$\boldsymbol{x}_k=\boldsymbol{P}_{n_k}(\boldsymbol{x}_{k-1})=\boldsymbol{P}(\boldsymbol{x}_{k-1},-\boldsymbol{K}_{n_k}(\boldsymbol{x}_{k-1}-\boldsymbol{x}^*)).\tag{16}$$

Therefore, for some initial condition $\boldsymbol{x}_0$ in the neighborhood of the fixed point $\boldsymbol{x}^*$, we have

$$\boldsymbol{x}_k=\boldsymbol{P}_{n_k}\circ\boldsymbol{P}_{n_{k-1}}\circ\ldots\circ\boldsymbol{P}_{n_1}(\boldsymbol{x}_0).\tag{17}$$

Now, the expression of $\boldsymbol{x}_k$ under feedback controller (11) has been derived, and the stabilization of the periodic gait is transformed into a problem of designing the feedback gains in each step such that

$$\lim_{k\to\infty}\boldsymbol{x}_k=\boldsymbol{x}^*.\tag{18}$$

2. Design of feedback gains

We present an adaptive control law to update the feedback gain in each step. First, a set of feedback gains are designed according to the discrete linear quadratic regulator (DLQR), where each feedback gain $\boldsymbol{K}_m$ ($m=1,2,\ldots$) is designed so that the

state feedback law $\boldsymbol{\beta}_k = -\boldsymbol{K}_m(\boldsymbol{x}_{k-1}-\boldsymbol{x}^*)$ minimizes the cost function $\sum_k(\delta\boldsymbol{x}_{k-1}^{\mathrm{T}}Q\delta\boldsymbol{x}_{k-1}+\boldsymbol{\beta}_k^{\mathrm{T}}R\boldsymbol{\beta}_k)$ subject to the state dynamics $\delta\boldsymbol{x}_k = \boldsymbol{A}\delta\boldsymbol{x}_{k-1}+\boldsymbol{F}\boldsymbol{\beta}_k$, which is the linearization of Eq. (14). Here, $\boldsymbol{A}$ is the Jacobian of $\boldsymbol{P}$ at the fixed point $\boldsymbol{x}^*$, $\boldsymbol{F}$ is the Jacobian of $\boldsymbol{P}$ with respect to $\boldsymbol{\beta_k}$, $\delta\boldsymbol{x}_{k-1} = \boldsymbol{x}_{k-1}-\boldsymbol{x}^*$, and Q and R are the real positive weighting coefficients associated with the convergence rate and input energy, respectively. In this study, four feedback gains are designed in terms of the tradeoff between the convergence rate and input energy (Table 1). Moreover, for each feedback gain $\boldsymbol{K}_m$ designed by the DLQR method, the eigenvalues of the Poincaré map $\boldsymbol{P}_m$ will have a magnitude strictly less than one. Then from Westervelt et al. (2007), there exists a small constant $r>0$ such that for any initial condition $\boldsymbol{x}_0 \in \boldsymbol{B}(\boldsymbol{x}^*, r)$, where $\boldsymbol{B}(\boldsymbol{x}^*, r) = \{\boldsymbol{z} | \parallel \boldsymbol{z}-\boldsymbol{x}^* \parallel < r\}$, we have

$$\lim_{k\to\infty} \boldsymbol{P}_m^k(\boldsymbol{x}_0) = \boldsymbol{x}^*, \tag{19}$$

where $\boldsymbol{P}_m^k$ is the k^{th} iteration of $\boldsymbol{P}_m$ from $\boldsymbol{x}_0$.

Table 1 Different feedback gains with different weighting coefficients

$\boldsymbol{K}_1$	$\boldsymbol{K}_2$	$\boldsymbol{K}_3$	$\boldsymbol{K}_4$
$Q=1$ $R=2$	$Q=1$ $R=1$	$Q=1\times10^2$ $R=1\times10^{-2}$	$Q=1\times10^4$ $R=1\times10^{-4}$

Next, we present an adaptive algorithm to pick out the feedback gains in each step. Consider the feedback gains $\boldsymbol{K}_1$ and $\boldsymbol{K}_2$, and suppose that there exists a sufficiently small constant $r>0$ such that for any initial condition $\boldsymbol{x}_0 \in \boldsymbol{B}(\boldsymbol{x}^*, r)$, $\lim_{k\to\infty}\boldsymbol{P}_1^k(\boldsymbol{x}_0) = \boldsymbol{x}^*$ and $\lim_{k\to\infty}\boldsymbol{P}_2^k(\boldsymbol{x}_0) = \boldsymbol{x}^*$. If there exists a positive integer n such that $\parallel \boldsymbol{P}_1^n(\boldsymbol{x}_0)-\boldsymbol{x}^* \parallel \le \parallel \boldsymbol{x}_0-\boldsymbol{x}^* \parallel$, then it can be easily deduced that

$$\lim_{k\to\infty} \boldsymbol{P}_2^k(\boldsymbol{P}_1^n(\boldsymbol{x}_0)) = \boldsymbol{x}^*. \tag{20}$$

Eq. (20) shows that a periodic gait can be stabilized by a combination of different feedback gains under certain conditions. Based on this observation, we present an adaptive algorithm to pick out the feedback gains in each step to achieve an optimal performance in terms of the balance between the convergence rate and input energy. In the first few walking steps, where large state errors may exist, the feedback gains are chosen with an emphasis on the input torque, whereas in the successive walking steps, the feedback gains are chosen to have a fast convergence rate. The algorithm is summarized in Algorithm 1, where ϵ is a positive constant, which is set to be 5×10^{-2} here. Based on this algorithm, the state $\boldsymbol{x}_k$ in Eq. (17) becomes

$$\boldsymbol{x}_k = \boldsymbol{P}_4^{k_4}\circ\boldsymbol{P}_3^{k_3}\circ\boldsymbol{P}_2^{k_2}\circ\boldsymbol{P}_1^{k_1}(\boldsymbol{x}_0), \tag{21}$$

where k_1, k_2, k_3, and k_4 are nonnegative integers and $k_1+k_2+k_3+k_4=k$. Because $\parallel \boldsymbol{x}_k \parallel < \parallel \boldsymbol{x}_{k-1} \parallel$ holds in each step, it is easy to deduce that $\lim_{k\to\infty}\boldsymbol{x}_k = \boldsymbol{x}^*$. Therefore, the closed-loop system is stable.

Algorithm 1 Update of the feedback gain in each step

Input: State $\boldsymbol{x}_{k-1}$ and n_k with $n_1=1$
1: $\boldsymbol{x}_k = \boldsymbol{P}_{n_k}(\boldsymbol{x}_{k-1})$, $\delta\boldsymbol{x}_{k-1} = \boldsymbol{x}_{k-1}-\boldsymbol{x}^*$, $\delta\boldsymbol{x}_k = \boldsymbol{x}_k-\boldsymbol{x}^*$
2: Let $m=n_k$ and $\boldsymbol{\beta}_{k+1} = \boldsymbol{K}_{m+1}\delta\boldsymbol{x}_k$
3: **while** $m<4$ **do**
4: **if** $\parallel \boldsymbol{x}_k \parallel < \parallel \boldsymbol{x}_{k-1} \parallel$ and $\parallel \boldsymbol{\beta}_{k+1} \parallel < \epsilon$ **then**
5: $m=m+1$
6: **else**
7: $m=m$
8: break
9: **end if**
10: **end while**
11: $n_{k+1}=m$
Output: $\boldsymbol{K}_{n_{k+1}}$, the feedback gain in step $k+1$

3.3 Transition controller design

The design objective of the transition controller is to guide the biped from gait 2 to a neighboring point of the final state of gait 1 so that the state trajectory can smoothly converge to gait 1. Compared with previous works, the transition controller here takes into account the physical constraints in the transition process to guarantee a feasible gait transition. To achieve this goal, the transition controller is parameterized and designed as follows:

$$\begin{aligned}\boldsymbol{u}_{\mathrm{T}}(\boldsymbol{x}_1,\boldsymbol{\xi}) = {}& \boldsymbol{u}_{\mathrm{T}}^*(\boldsymbol{x}_1,\boldsymbol{\xi}) - (\boldsymbol{L}_{g_1}\boldsymbol{L}_{f_1}\boldsymbol{y}_{\mathrm{T}}(\boldsymbol{x}_1,\boldsymbol{\xi}))^{-1}\\ & \cdot\left(\frac{K_P}{\varepsilon^2}\boldsymbol{y}_{\mathrm{T}}(\boldsymbol{x}_1,\boldsymbol{\xi})+\frac{K_D}{\varepsilon}\dot{\boldsymbol{y}}_{\mathrm{T}}(\boldsymbol{x}_1,\boldsymbol{\xi})\right),\end{aligned} \tag{22}$$

where

$$\boldsymbol{u}_{\mathrm{T}}^*(\boldsymbol{x}_1,\boldsymbol{\xi}) = -(\boldsymbol{L}_{g_1}\boldsymbol{L}_{f_1}\boldsymbol{y}_{\mathrm{T}}(\boldsymbol{x}_1,\boldsymbol{\xi}))^{-1}\boldsymbol{L}_{f_1}^2\boldsymbol{y}_{\mathrm{T}}(\boldsymbol{x}_1,\boldsymbol{\xi}),$$

and $\boldsymbol{y}_{\mathrm{T}}(\boldsymbol{x}_1,\boldsymbol{\xi})$ is the output of the transitional control with a vector of control parameters $\boldsymbol{\xi}$, which is

designed as

$$\boldsymbol{y}_{\mathrm{T}}(\boldsymbol{x}_1,\boldsymbol{\xi})=\boldsymbol{q}_a-\underbrace{(\boldsymbol{h}_{\mathrm{T}}(\theta)+\boldsymbol{h}_m(\theta,\boldsymbol{\xi}))}_{\boldsymbol{h}_{\mathrm{d,T}}}. \tag{23}$$

Here, $\boldsymbol{h}_{\mathrm{d,T}}$ denotes the evolution of the controlled joints for the transition process that connects the initial state of gait 2 and some neighboring point of the final state of gait 1, $\boldsymbol{h}_{\mathrm{T}}(\boldsymbol{\xi})$ is the third-order Bezier polynomial of $\boldsymbol{\xi}$, the Bezier coefficients are determined from $(\boldsymbol{x}^+)_2$ and $(\boldsymbol{x}^-)_1$ (Fig. 2), and $\boldsymbol{h}_m(\theta,\boldsymbol{\xi})$ is designed to be a fifth-order polynomial of θ such that

$$\begin{cases}\boldsymbol{h}_m((\theta_{\mathrm{ini}})_2,\boldsymbol{\xi})=\boldsymbol{0},\\ \dfrac{\partial\boldsymbol{h}_m}{\partial\theta}((\theta_{\mathrm{ini}})_2,\boldsymbol{\xi})=\boldsymbol{0},\\ \boldsymbol{h}_m(((\theta_{\mathrm{ini}})_2+(\theta_{\mathrm{f}})_1)/2,\boldsymbol{\xi})=\boldsymbol{\xi},\\ \boldsymbol{h}_m((\theta_{\mathrm{f}})_1,\boldsymbol{\xi})=\boldsymbol{0},\end{cases} \tag{24}$$

in which $(\theta_{\mathrm{ini}})_2$ is the desired initial value of θ for gait 2 and $(\theta_{\mathrm{f}})_1$ is the desired final value of θ for gait 1. Moreover, the values of both the velocity and acceleration of $\boldsymbol{h}_m(\theta,\boldsymbol{\xi})$ are set to be $\boldsymbol{0}$ at $\theta=(\theta_{\mathrm{f}})_1$.

To guarantee the physical constraints for bipedal walking and guide the biped to a neighboring point of the final state of gait 1, the parameter $\boldsymbol{\xi}$ is obtained by solving the following optimization problem: find the six optimization parameters that prescribe a parameter vector $\boldsymbol{\xi}$ that minimizes the cost function

$$J_{\mathrm{T}}=\boldsymbol{\xi}^{\mathrm{T}}\boldsymbol{\xi} \tag{25}$$

subject to the physical constraints and the final state constraint:

$$\left\|[(q_{2,\mathrm{f}})_1,(\dot{\theta}_{\mathrm{f}})_1,(\dot{q}_{2,\mathrm{f}})_1]^{\mathrm{T}}-[q_2(t_{\mathrm{f}}),\theta(t_{\mathrm{f}}),\dot{q}_2(t_{\mathrm{f}})]^{\mathrm{T}}\right\|<\delta, \tag{26}$$

where $(q_{2,\mathrm{f}})_1$ denotes the desired final value of q_2, $q_2(t)$ and $\theta(t)$ result from the integration of the dynamic model (7), the duration t_{f} satisfies $\theta(t_{\mathrm{f}})=(\theta_{\mathrm{f}})_1$, and δ is a positive threshold indicating the distance between the transition trajectory and gait 1, which is set to be 1×10^{-2} here. The above optimization process is also performed with the Patternsearch function in the optimization toolbox, and the termination tolerance is set to be δ.

4 Numerical simulation

In this section, we present a numerical example to verify the control strategy developed in Section 3. The 3D bipedal robot is shown in Fig. 1 and the structural parameters of the robot are from Chevallereau et al. (2009). To implement the gait transition control strategy, we consider two gaits with different step lengths. The desired final states for gait 1 and gait 2 are denoted as $(\boldsymbol{x}^-)_1=[(\boldsymbol{q}^-)_1,(\dot{\boldsymbol{q}}^-)_1]^{\mathrm{T}}$ and $(\boldsymbol{x}^-)_2=[(\boldsymbol{q}^-)_2,(\dot{\boldsymbol{q}}^-)_2]^{\mathrm{T}}$, respectively, and

$$\begin{aligned}(\boldsymbol{q}^-)_1=&[-0.3275,-0.0264,0.3896,-0.2968,\\&0.0618,0.0331,-0.5002,0.2097]^{\mathrm{T}},\\(\dot{\boldsymbol{q}}^-)_1=&[-1.2051,-0.4856,0.0941,0.8526,\\&0.1447,0.3983,2.0159,-2.9982]^{\mathrm{T}},\\(\boldsymbol{q}^-)_2=&[-0.3067,-0.0258,0.3644,-0.2819,\\&0.0480,0.0161,-0.4937,0.2323]^{\mathrm{T}},\\(\dot{\boldsymbol{q}}^-)_2=&[-1.2132,-0.4565,0.0923,1.0970,\\&0.1255,0.3955,2.0201,-3.0]^{\mathrm{T}}.\end{aligned}$$

The step lengths for gait 1 and gait 2 are 0.16 m and 0.15 m, respectively. In the following, the presented strategy is applied to realize a smooth transition from gait 2 to gait 1. The same method can be applied for the transition between other gaits in a gait library.

According to Section 3.2, a set of feedback gains are first designed according to the DLQR method. The three largest eigenvalues under the feedback gains are given in Table 2; their magnitudes are all less than one. To verify the controller, the 3D biped's dynamic model in a closed loop is simulated with an initial state slightly perturbed from the desired final state $(\boldsymbol{x}^-)_1$. A velocity deviation of 0.03 rad/s is introduced on each joint. We say the robot converges to the limit cycle if the modulus of the error $\|\boldsymbol{x}_1-(\boldsymbol{x}^-)_1\|$ is less than 2×10^{-6}. As a comparison, we consider the event-based controllers with constant feedback gain $\boldsymbol{K}_1$ (the most efficient) and $\boldsymbol{K}_4$ (the most rapid convergence). Fig. 3 shows the phase portraits for q_i ($i=5,\ 6,\ 7,\ 8$). Under the controller with constant gain $\boldsymbol{K}_1$, the state trajectory converges to the desired gait in 12 steps, whereas under the controller with constant gain $\boldsymbol{K}_4$ and the present controller, the state trajectory converges to the desired gait in five steps. Fig. 4 shows the torques in the first five walking steps. Under the controller with constant gain $\boldsymbol{K}_4$, the torques obviously have larger magnitudes, whereas the torques required for the present controller are nearly the same as those required for the controller with

constant gain $\boldsymbol{K}_1$. Therefore, compared with the customary event-based controllers with a constant feedback gain, the present controller exhibits an optimal performance in terms of the balance between the convergence rate and input torques.

Table 2 Three largest eigenvalues under different feedback gains

Feedback gain	Three largest eigenvalues		
$\boldsymbol{K}_1$	0.4282	–0.2931	–0.2086
$\boldsymbol{K}_2$	0.3130	–0.3093	–0.1922
$\boldsymbol{K}_3$	–0.4331	0.0005	–0.0001
$\boldsymbol{K}_4$	–0.0177	0	0
Without feedback	–3.8155	0.8923	–0.2408

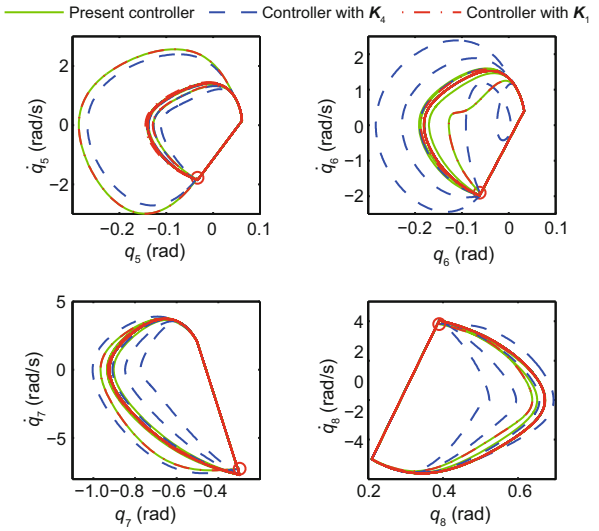

Fig. 3 Phase portraits for q_i ($i = 5, 6, 7, 8$), where the initial condition is represented by a circle. Under the present controller and the controllers with constant gains $\boldsymbol{K}_1$ and $\boldsymbol{K}_4$, the robot converges to the desired gait in 5, 12, and 5 steps, respectively

Next, to achieve a smooth transition, a transition controller is designed by following the method in Section 3.3, and the controller parameter $\boldsymbol{\xi}$ is obtained as $\boldsymbol{\xi} = [-0.0377, -0.0510, -0.0487, 0.0191, 0.0926, -0.0054]^{\mathrm{T}}$. As shown in Fig. 5, under the transition controller, the walking of the biped successfully transited from gait 2 to gait 1 in six steps. Fig. 6 shows the torques required to realize the transition. As a comparison, the torques for the gait transition without the transition controller are presented. The results show that, under the transition controller, the peak value of the torques is reduced by 43%.

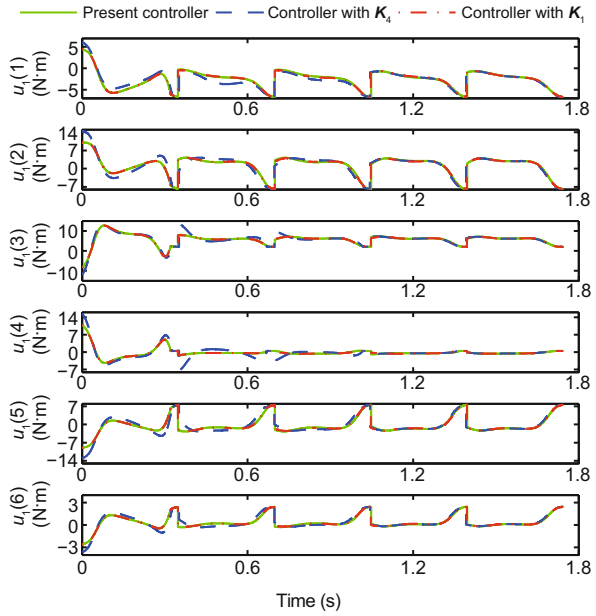

Fig. 4 Torques required for the three controllers in the first five walking steps

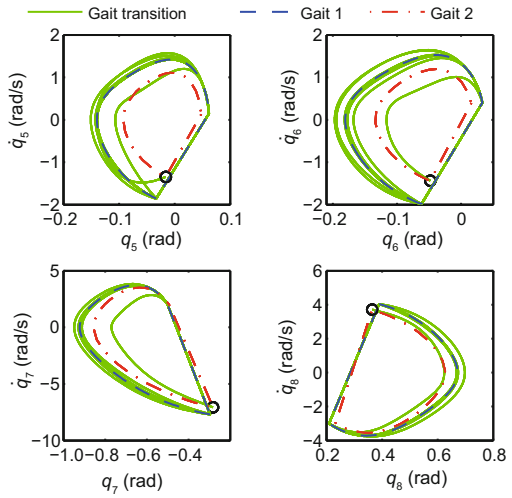

Fig. 5 Phase portraits under gait transition, where the initial condition is represented by a circle, and the walking of the robot transited from gait 2 to gait 1 in six steps

5 Conclusions and future work

We studied the gait transition problem of a five-link underactuated 3D bipedal robot, and proposed a two-layer control strategy that consists of an event-based feedback controller and a transition controller. Compared with a customary event-based feedback controller with a constant feedback gain, the feedback gain of the present controller in each step was updated by an adaptive control law. To guarantee the physical constraints in the transition process,

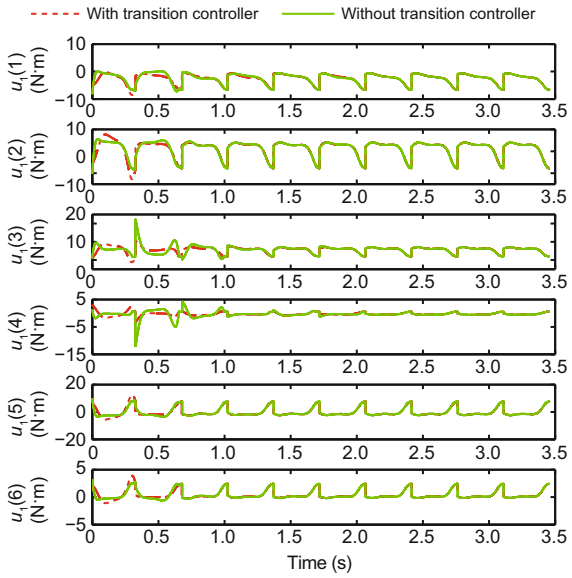

Fig. 6 Torques required for gait transition. The peak values of the torques with and without the transition controller are 12.5 and 22.1 N·m, respectively

the transition controller was parameterized and its control parameters were obtained by solving an optimization problem. The validity and effectiveness of the control strategy were illustrated by a numerical simulation.

In this paper, we simply used the actuated joints as the controlled variables for the output of the controller. In future research, we will consider improving the stability of the controller by making a proper choice of the output. It would also be very interesting to extend the presented control strategy to fully actuated bipedal robots with underactuated walking phases to achieve robust dynamic walking under various kinds of disturbances.

Compliance with ethics guidelines

Hai-hui YUAN, Yi-min GE, and Chun-biao GAN declare that they have no conflict of interest.

References

Ames AD, 2014. Human-inspired control of bipedal walking robots. *IEEE Trans Autom Contr*, 59(5):1115-1130. https://doi.org/10.1109/TAC.2014.2299342

Ames AD, Galloway K, Sreenath K, et al., 2014. Rapidly exponentially stabilizing control Lyapunov functions and hybrid zero dynamics. *IEEE Trans Autom Contr*, 59(4):876-891. https://doi.org/10.1109/TAC.2014.2299335

Chevallereau C, Grizzle JW, Shih CL, 2009. Asymptotically stable walking of a five-link underactuated 3D bipedal robot. *IEEE Trans Rob*, 25(1):37-50. https://doi.org/10.1109/TRO.2008.2010366

Collins S, Ruina A, Tedrake R, et al., 2005. Efficient bipedal robots based on passive-dynamic walkers. *Science*, 307(5712):1082-1085. https://doi.org/10.1126/science.1107799

Da XY, Harib O, Hartley R, et al., 2016. From 2D design of underactuated bipedal gaits to 3D implementation: walking with speed tracking. *IEEE Access*, 4:3469-3478. https://doi.org/10.1109/ACCESS.2016.2582731

Da XY, Hartley R, Grizzle JW, 2017. Supervised learning for stabilizing underactuated bipedal robot locomotion, with outdoor experiments on the wave field. IEEE Int Conf on Robotics and Automation, p.3476-3483. https://doi.org/10.1109/ICRA.2017.7989397

Dehghani R, Fattah A, Abedi E, 2015. Cyclic gait planning and control of a five-link biped robot with four actuators during single support and double support phases. *Multibody Syst Dynam*, 33(4):389-411. https://doi.org/10.1007/s11044-013-9404-5

Freidovich LB, Mettin U, Shiriaev AS, et al., 2009. A passive 2-DOF walker: hunting for gaits using virtual holonomic constraints. *IEEE Trans Rob*, 25(5):1202-1208. https://doi.org/10.1109/TRO.2009.2028757

Geng T, 2014. Online regulation of the walking speed of a planar limit cycle walker via model predictive control. *IEEE Trans Ind Electron*, 61(5):2326-2333. https://doi.org/10.1109/TIE.2013.2272274

Gregg RD, Righetti L, 2013. Controlled reduction with unactuated cyclic variables: application to 3D bipedal walking with passive yaw rotation. *IEEE Trans Autom Contr*, 58(10):2679-2685. https://doi.org/10.1109/TAC.2013.2256011

Griffin B, Grizzle J, 2017. Nonholonomic virtual constraints and gait optimization for robust walking control. *Int J Rob Res*, 36(8):895-922. https://doi.org/10.1177/0278364917708249

Grizzle JW, Abba G, Plestan F, 2001. Asymptotically stable walking for biped robots: analysis via systems with impulse effects. *IEEE Trans Autom Contr*, 46(1):51-64. https://doi.org/10.1109/9.898695

Grizzle JW, Chevallereau C, Sinnet RW, et al., 2014. Models, feedback control, and open problems of 3D bipedal robotic walking. *Automatica*, 50(8):1955-1988. https://doi.org/10.1016/j.automatica.2014.04.021

Hamed KA, Grizzle JW, 2014. Event-based stabilization of periodic orbits for underactuated 3D bipedal robots with left-right symmetry. *IEEE Trans Rob*, 30(2):365-381. https://doi.org/10.1109/TRO.2013.2287831

Hamed KA, Buss BG, Grizzle JW, 2016. Exponentially stabilizing continuous-time controllers for periodic orbits of hybrid systems: application to bipedal locomotion with ground height variations. *Int J Rob Res*, 35(8):977-999. https://doi.org/10.1177/0278364915593400

Hirose M, Ogawa K, 2007. Honda humanoid robots development. *Phil Trans R Soc A*, 365(1850):11-19. https://doi.org/10.1098/rsta.2006.1917

Hobbelen DGE, Wisse M, 2008. Controlling the walking speed in limit cycle walking. *Int J Rob Res*, 27(9):989-1005. https://doi.org/10.1177/0278364908095005

Hu Y, Yan GF, Lin ZY, 2011. Feedback control of planar biped robot with regulable step length and walking speed. *IEEE Trans Rob*, 27(1):162-169. https://doi.org/10.1109/TRO.2010.2085471

Kaneko K, Kanehiro F, Morisawa M, et al., 2011. Humanoid robot HRP-4—humanoid robotics platform with lightweight and slim body. IEEE/RSJ Int Conf on Intelligent Robots and Systems, p.4400-4407. https://doi.org/10.1109/IROS.2011.6094465

Kaneko K, Morisawa M, Kajita S, et al., 2015. Humanoid robot HRP-2Kai—improvement of HRP-2 towards disaster response tasks. Proc 15th Int Conf on Humanoid Robots, p.132-139. https://doi.org/10.1109/HUMANOIDS.2015.7363526

Li C, Xiong R, Zhu QG, et al., 2015. Push recovery for the standing under-actuated bipedal robot using the hip strategy. *Front Inform Technol Electron Eng*, 16(7):579-593. https://doi.org/10.1631/FITEE.14a0230

Montano O, Orlov Y, Aoustin Y, et al., 2017. Orbital stabilization of an underactuated bipedal gait via nonlinear H_∞-control using measurement feedback. *Auton Rob*, 41(6):1277-1295. https://doi.org/10.1007/s10514-015-9543-z

Moon JS, Stipanovic DM, Spong MW, 2016. Gait generation and stabilization for nearly passive dynamic walking using auto-distributed impulses. *Asian J Contr*, 18(4):1343-1358. https://doi.org/10.1002/asjc.1206

Nguyen Q, Agrawal A, Da XY, 2017. Dynamic walking on randomly-varying discrete terrain with one-step preview. In: Robotics: Science and Systems. Cambridge, MA, USA.

Park IW, Kim JY, Lee J, et al., 2007. Mechanical design of the humanoid robot platform, HUBO. *Adv Rob*, 21(11):1305-1322. https://doi.org/10.1163/156855307781503781

Shih CL, Grizzle J, Chevallereau C, 2012. From stable walking to steering of a 3D bipedal robot with passive point feet. *Robotica*, 30(7):1119-1130. https://doi.org/10.1017/S026357471100138X

Sreenath K, Park HW, Poulakakis I, et al., 2013. Embedding active force control within the compliant hybrid zero dynamics to achieve stable, fast running on MABEL. *Int J Rob Res*, 32(3):324-345. https://doi.org/10.1177/0278364912473344

Tang C, Yan GF, Lin ZY, et al., 2015. Stable walking of 3D compass-like biped robot with underactuated ankles using discrete transverse linearization. *Trans Inst Meas Contr*, 37(9):1074-1083. https://doi.org/10.1177/0142331214555895

Vukobratović M, Borovac B, 2004. Zero-moment point—thirty five years of its life. *Int J Humanoid Rob*, 1(1):157-173. https://doi.org/10.1142/S0219843604000083

Westervelt ER, Grizzle JW, Chevallereau C, et al., 2007. Feedback Control of Dynamic Bipedal Robot Locomotion. CRC Press, Boca Raton, USA.

Yanco HA, Norton A, Ober W, et al., 2015. Analysis of human-robot interaction at the DARPA robotics challenge trials. *J Field Rob*, 32(3):420-444. https://doi.org/10.1002/rob.21568

Yang T, Westervelt E, Serrani A, et al., 2009. A framework for the control of stable aperiodic walking in underactuated planar bipeds. *Auton Rob*, 27(3):277-290. https://doi.org/10.1007/s10514-009-9126-y

Yi Y, Lin ZY, 2015. Stability and agility: biped running over varied and unknown terrain. *Front Inform Technol Electron Eng*, 16(4):283-292. https://doi.org/10.1631/FITEE.1400284

Yi Y, Lin ZY, Yan GF, 2014. Variable speed running on kneed biped robot with underactuation degree two. *Int J Humanoid Rob*, 11(2):1450015. https://doi.org/10.1142/S0219843614500157